

# Quantum reflection of antihydrogen from the Casimir potential above matter slabs

G. Dufour,<sup>1</sup> A. Gérardin,<sup>1</sup> R. Guéroul,<sup>1</sup> A. Lambrecht,<sup>1</sup> V. V. Nesvizhevsky,<sup>2</sup> S. Reynaud,<sup>1</sup> and A. Yu. Voronin<sup>3</sup>

<sup>1</sup>*Laboratoire Kastler-Brossel, CNRS, ENS, UPMC, Campus Jussieu, F-75252 Paris, France*

<sup>2</sup>*Institut Laue-Langevin (ILL), 6 Rue Jules Horowitz, F-38042, Grenoble, France*

<sup>3</sup>*P. N. Lebedev Physical Institute, 53 Leninsky Prospect, Ru-117924 Moscow, Russia*

(Received 26 September 2012; published 2 January 2013)

We study quantum reflection of antihydrogen atoms from matter slabs due to the van der Waals–Casimir-Polder potential. By taking into account the specificities of antihydrogen and the optical properties and width of the slabs, we calculate realistic estimates for the potential and quantum reflection amplitudes. Next we discuss the paradoxical result of larger reflection coefficients estimated for weaker potentials in terms of the Schwarzian derivative. We analyze the limiting case of reflections at small energies, which are characterized by a scattering length and have interesting applications for trapping and guiding antihydrogen using material walls.

DOI: [10.1103/PhysRevA.87.012901](https://doi.org/10.1103/PhysRevA.87.012901)

PACS number(s): 34.35.+a, 36.10.Gv, 12.20.Ds

## I. INTRODUCTION

Quantum reflection is the process of reflection of particles from an attractive but rapidly varying potential. It has been studied since the early days of quantum theory [1]. On the other hand, it is well known that atoms in the vicinity of a surface experience the long-range van der Waals–Casimir-Polder (vdW-CP) potential [2]. Quantum reflection occurs here if the atom enters a region where the potential varies rapidly compared with the atom’s wavelength. Experimentally, quantum reflection on the vdW-CP potential has been observed with slow atoms reflected from a liquid helium surface [3–5] or from solid surfaces [6,7]. More recent efforts have focused on quantum reflection from rough or micro- and nanostructured surfaces [8–10] and on quantum reflection of Bose-Einstein condensates on flat or nanostructured silicon [11,12].

The theoretical description of quantum reflection has been the topic of numerous contributions in the past [13–18], which are presented in some detail in [19]. The particular case of reflection on a vdW-CP potential created by thin slabs or graphene sheets has been reported recently in [20]. In addition it has been put forward that quantum reflection coefficients can be tuned using external optical fields [21] or via thermal nonequilibrium effects [22].

In the present paper, we will study the quantum reflection of antihydrogen atoms  $\bar{\text{H}}$  falling on material walls. As  $\bar{\text{H}}$  atoms are annihilated in contact with matter, this case enforces specific boundary conditions at the material surface [23]. In particular, the behavior of the short-range atom-wall potential becomes irrelevant as all antiatoms that come close enough to the surface are annihilated. This topic is important to the GBAR Collaboration which aims to measure the gravitational behavior of  $\bar{\text{H}}$  by studying its time of free fall from a well-defined trap to a matter plate [24]. We will give accurate estimations for the van der Waals–Casimir-Polder potential between the antiatoms and the surface as well as for the associated quantum reflection.

A number of different methods are available to calculate atom-surface dispersion forces [25–28] (see [29] for a detailed bibliography). Here we will use the scattering approach [30,31] which has been developed to calculate Casimir forces in arbitrary geometries and which can be applied to the study

of vdW-CP forces between an atom and flat or nanostructured surfaces [32]. In order to obtain accurate estimations, it will in particular be necessary to take into account the material properties and the finite thickness of the slabs [33].

In order to explain the paradoxical result that larger reflections are obtained for weaker potentials, we will discuss how the quantum reflection occurs when the atoms approach the surface and draw a relation to the Schwarzian derivative. We will finally analyze the limiting case of reflections at small energies, which have interesting applications for trapping and guiding antihydrogen with material walls [34,35]. Quantum reflection is characterized by a scattering length which we will calculate for different materials and different slab widths. We note at this point that quantum reflection is calculated in the present paper from a static potential, so that the role of dissipation in matter is neglected [36].

## II. CASIMIR-POLDER POTENTIAL

We use the scattering formalism [30,31] applied here to the Casimir-Polder potential between an atom and a plate:

$$V(z) = \hbar \int_0^\infty \frac{d\xi}{2\pi} \text{Tr} \ln(1 - \mathcal{R}_P e^{-\kappa z} \mathcal{R}_A e^{-\kappa z}). \quad (1)$$

As the quantum reflection process is expected to occur at distances smaller than 1  $\mu\text{m}$  (more discussion is given below), and thus smaller than the typical thermal wavelength, this formula has been written at zero temperature. The matrices  $\mathcal{R}_P$  and  $\mathcal{R}_A$  describe the reflection of the electromagnetic vacuum fields on the plate and atom, respectively. They are calculated for a Wick-rotated complex frequency  $\omega = i\xi$  with the trace (Tr) bearing on transverse wave vectors  $\mathbf{k}$  and polarizations  $p = \text{TE, TM}$ . The factor  $e^{-\kappa z}$  accounts for propagation between the atom and plate where  $\kappa = \sqrt{\mathbf{k}^2 + \xi^2/c^2}$  is the Wick-rotated complex longitudinal wave vector.

We may safely neglect all multiple reflections between the atom and the surface and thus expand the general scattering formula (1) to first order in  $\mathcal{R}_A$ . When the scattering on the atom is described in the dipolar approximation [32], the potential is read in terms of a dynamic atomic polarizability

$\alpha$ , given in units of a volume:

$$V(z) = \frac{\hbar}{c^2} \int_0^\infty d\xi \xi^2 \alpha(i\xi) \int \frac{d^2\mathbf{k}}{(2\pi)^2} \frac{e^{-2\kappa z}}{\kappa} \times \left[ \rho^{\text{TE}} - \left( 1 + \frac{2c^2 k^2}{\xi^2} \right) \rho^{\text{TM}} \right]. \quad (2)$$

The  $\rho^p$  denote the electromagnetic reflection amplitudes for the two polarizations  $p = \text{TE}, \text{TM}$ . We study first the case of reflection from a semi-infinite bulk, described by the Fresnel laws expressing continuity relations at the interface:

$$\rho_{\text{bulk}}^{\text{TE}} = \frac{\kappa - K}{\kappa + K}, \quad \rho_{\text{bulk}}^{\text{TM}} = \frac{\epsilon(i\xi)\kappa - K}{\epsilon(i\xi)\kappa + K}, \quad (3)$$

where  $K = \sqrt{\mathbf{k}^2 + \epsilon(i\xi)(\xi/c)^2}$  corresponds to the Wick-rotated longitudinal wave vector inside the medium, and  $\epsilon$  is the relative dielectric function of this medium (evaluated at the Wick-rotated complex frequency).

The results presented below use the following optical response properties:

- (1) The atomic polarizability is that of antihydrogen ( $\bar{\text{H}}$ ), and is assumed to be the same as that of hydrogen (H) [37].
- (2) Perfect mirrors have been used in previous calculations [18,23,37]

$$\rho^{\text{TE}} \equiv -1, \quad \rho^{\text{TM}} \equiv 1; \quad (4)$$

they are considered here for the sake of comparison with results obtained with the real materials discussed below.

- (3) Mirrors made of intrinsic silicon are described by a Drude-Lorentz model [32,33]:

$$\epsilon(i\xi) = \epsilon_\infty + \frac{(\epsilon_0 - \epsilon_\infty)\omega_0^2}{\xi^2 + \omega_0^2}, \quad (5)$$

with the parameters  $\epsilon_0 = 11.87$ ,  $\epsilon_\infty = 1.035$ , and  $\omega_0 = 6.6 \times 10^{15} \text{ rad s}^{-1}$ .

- (4) Mirrors made of amorphous silica are described by a simple Sellmeier model [38]:

$$\epsilon(i\xi) = 1 + \sum_{i=1,2,3} \frac{B_i}{1 + (\xi/\omega_i)^2}, \quad (6)$$

with the parameters  $B_{1,2,3} = 0.696749, 0.408218, \text{ and } 0.890815$  and  $\omega_{1,2,3} = 27.2732 \times 10^{15}, 16.2858 \times 10^{15}, \text{ and } 0.190257 \times 10^{15} \text{ rad s}^{-1}$ .

- (5) The electronic properties of graphene are described by a Dirac model leading to the reflection coefficients given in [39].

The potential (2) has well-known asymptotic behaviors at short and long distances,

$$V(z) \xrightarrow{z \ll \ell} -\frac{C_3}{z^3}, \quad V(z) \xrightarrow{z \gg \ell} -\frac{C_4}{z^4}, \quad (7)$$

where  $\ell$  is a distance scale determined by the characteristic atomic frequencies which enter the expressions for the polarizability or dielectric function. The short-distance limit is identical to the famous London–van der Waals result while the long-distance limit is the so-called *retarded* Casimir-Polder interaction which takes into account that the finite speed of light comes into play at large separations [2]. The values given in Table I are obtained from the exact vdW-CP potential (2) and given in atomic units.

TABLE I. Coefficients  $C_3$  and  $C_4$  for the vdW-CP interaction for  $\bar{\text{H}}$  atoms above perfect mirrors and bulk silicon and silica; the values are given in atomic units  $E_h a_0^n$  for  $C_n$  (Hartree energy  $E_h \simeq 4.3597 \text{ aJ}$ ; Bohr radius  $a_0 \simeq 52.917 \text{ pm}$ ).

	Perfect mirror	Silicon	Silica
$C_3$	0.25	0.10	0.05
$C_4$	73.6	50.3	28.1

Figure 1 displays the exact vdW-CP potentials obtained from (2) for  $\bar{\text{H}}$  atoms on perfect mirrors and bulk mirrors made of intrinsic silicon or amorphous silica, described by Eqs. (4), (5), and (6), respectively. All cases are drawn as ratios  $V(z)/V^*(z)$  to the retarded CP limit calculated for a perfectly reflecting wall,  $V^* = -C_4^*/z^4$  with  $C_4^* = 2.5 \times 10^{-57} \text{ J m}^4$  ( $\simeq 73.6 \text{ a.u.}$ ; see Table I). The ratios tend to constant values  $C_4/C_4^*$  at large distances and linear variations  $C_3 z/C_4^*$  at small distances. Of course, lesser and lesser reflective materials produce weaker and weaker CP potentials, from perfect mirrors to silicon and silica plates.

### III. QUANTUM REFLECTION OF $\bar{\text{H}}$

We will now solve the problem of quantum reflection of  $\bar{\text{H}}$  atoms from the CP potential calculated in the previous section, starting from free atoms with an energy  $E > 0$  just before they feel the CP potential. We will also use below the notation  $h$  for the height of free fall of the atoms with the correspondence  $E = mgh$  (supposing  $h$  much larger than tens of microns).

The Schrödinger equation may be written

$$\psi''(z) + \frac{p^2(z)}{\hbar^2} \psi = 0, \quad (8)$$

where primes denote derivations with respect to  $z$  while  $p^2$  is the square of the semiclassical momentum

$$p(z) = \sqrt{2m[E - V(z)]}. \quad (9)$$

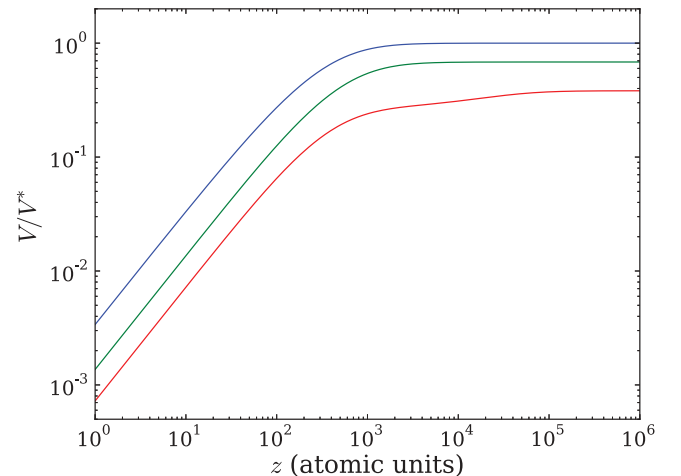


FIG. 1. (Color online) Casimir-Polder potential for  $\bar{\text{H}}$  in the vicinity of a bulk material, drawn as a ratio  $V/V^*$  with the retarded potential  $V^*$  for a perfect mirror; from top to bottom, perfect mirror (blue), silicon (green), and silica (red).

The general solution can be expressed, without approximation, as a superposition of the two WKB waves

$$\psi(z) = \frac{c_+(z)}{\sqrt{|p(z)|}} e^{i\phi(z)} + \frac{c_-(z)}{\sqrt{|p(z)|}} e^{-i\phi(z)}, \quad (10)$$

where  $\phi$  is the WKB phase ( $z_0$  arbitrary)

$$\phi(z) = \int_{z_0}^z \frac{p(z') dz'}{\hbar}. \quad (11)$$

The Schrödinger equation (8) is obeyed when the amplitudes  $c_{\pm}$  verify the coupled first-order equations [13]

$$c'_{\pm}(z) = e^{\mp 2i\phi(z)} \frac{p'(z)}{2p(z)} c_{\mp}(z). \quad (12)$$

As  $\bar{H}$  annihilates as soon as it touches the wall, there cannot be any wave reflected immediately from the surface  $z = 0$  of the material boundary [23]. This full absorption condition imposes  $c_+(z=0) = 0$  and we are then free to fix  $c_-(z=0) = 1$ . The quantum reflection amplitude  $r$  is thus given by the ratio of the amplitudes  $c_+(z)$  and  $c_-(z)$  at the limit  $z \rightarrow \infty$  [see Eq. (10)]. Finally, the quantum reflection probability discussed below is the squared modulus of this amplitude  $|r|^2$ .

In order to numerically integrate the preceding equations, it remains to fix the problems arising from the divergence of the potential in the vicinity of the surface. It will result from forthcoming discussions that the WKB waves are well defined near the wall. However, a difficulty arises from the divergence of the WKB phase  $\phi$  there. To fix this difficulty, we proceed as in [23] by studying the analytical form of the solution for  $c_{\pm}$  close enough to the wall. The potential there takes its van der Waals approximated form while the energy  $E$  becomes negligible when compared to the potential.

In this limit the functions  $f_{\pm}(t)$  defined by  $c_{\pm}(z) = x^{3/2} f_{\pm}(t)$ ,  $x = \sqrt{8mC_3/z}$ , and  $t = \pm 2ix$  satisfy the Kummer equation

$$t f_{\pm}''(t) + (b-t) f_{\pm}'(t) - a f_{\pm}(t) = 0 \quad (13)$$

with parameters  $a = 3/2$  and  $b = 4$ . A pair of independent solutions is given by Kummer's confluent hypergeometric functions  $M(a,b,t)$  and  $U(a,b,t)$  [40]. On the other hand, the Schrödinger equation (8) can also be solved close to the wall. The two counterpropagating waves can be expressed in terms of the Hankel functions as  $H_1^{(1)}(x)/x$  and  $H_1^{(2)}(x)/x$  and the full absorption condition imposes the requirement that the second wave has a null amplitude [23]. By comparing this expression of the wave function with (10) we find that

$$c_+(x) = -2(1+i)x^{3/2} \left[ U\left(\frac{3}{2}, 4, 2ix\right) - \frac{i\sqrt{\pi}}{8} M\left(\frac{3}{2}, 4, 2ix\right) \right] e^{-2ix_0}, \quad (14a)$$

$$c_-(x) = -2(1+i)x^{3/2} U\left(\frac{3}{2}, 4, -2ix\right). \quad (14b)$$

A better behavior of the functions is thus obtained by changing the variables  $z \rightarrow x$  in the vicinity of matter and matching the numerical solutions to the known analytical solutions (14). The results shown below are obtained in this manner close to the wall, while the variables are switched back to  $z$  when the potential becomes comparable to the energy.

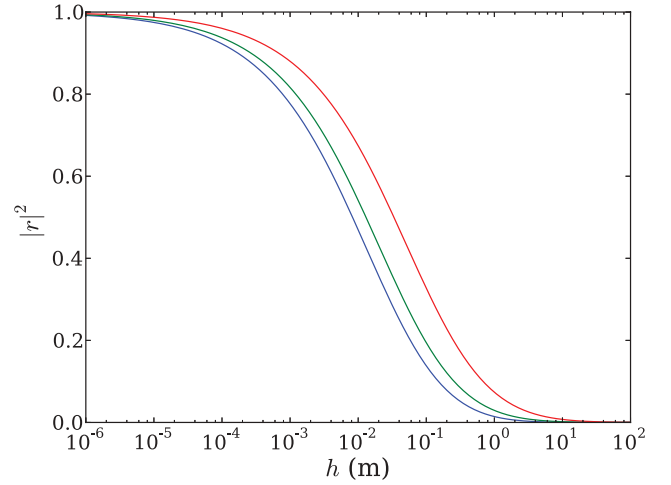


FIG. 2. (Color online) Quantum reflection probability  $|r|^2$  as a function of the free-fall height  $h$  for  $\bar{H}$  atoms on bulk mirrors; from bottom to top, perfect mirror (blue), silicon (green), and silica (red).

We show in Fig. 2 the numerical solutions for the quantum reflection probability obtained with the exact CP-vdW potentials discussed in the preceding section for  $\bar{H}$  atoms falling on perfect mirrors and bulk mirrors made of silicon or silica. It turns out that significant values are obtained for the quantum reflection probability with the typical numbers considered for the project GBAR as shown in Table II.

These numbers highlight a striking result of the calculations which is also emphasized by the use of the same color codes in Figs. 1 and 2: when going to less and less reflective materials, i.e., weaker and weaker CP-vdW interactions, one indeed obtains larger and larger quantum reflection probability [12,20]. This apparent paradox is analyzed in the next section, by taking a closer look at the region where quantum reflection occurs.

#### IV. BADLANDS CONDITION

We now discuss the so-called *badlands* condition for efficient reflection, that is, for significant nonadiabatic transitions beyond the WKB approximation [13,19]. With this aim, we recall that the WKB approximation  $\tilde{\psi}$ , the wavefunction (10) with constant amplitudes  $c_{\pm}$ , also obeys the Schrödinger equation

$$\tilde{\psi}''(z) + \frac{\tilde{p}^2(z)}{\hbar^2} \tilde{\psi}(z) = 0, \quad \tilde{p}^2(z) \equiv p^2(z) + \frac{\hbar^2}{2} \mathcal{S}\phi(z). \quad (15)$$

The difference between (8) and (15) is the extra term in  $\tilde{p}^2$  with respect to  $p^2$ , proportional to the Schwarzian derivative

TABLE II. Reflection probabilities for a free-fall height  $h \sim 10$  cm, which corresponds to an energy per unit mass  $gh \sim 1$  (m/s)<sup>2</sup> at the matter plate.

	Perfect mirror	Silicon	Silica
$ r ^2$	14%	20%	32%

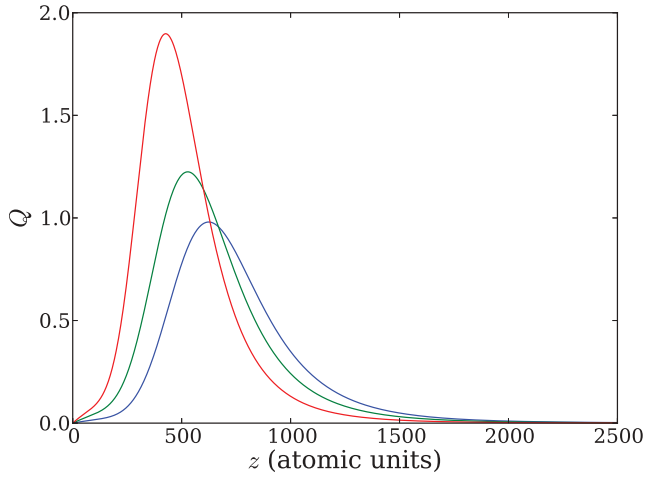


FIG. 3. (Color online) Badlands function  $Q(z)$  as a function of distance to the wall (atomic units) for  $\bar{H}$  dropped from  $h = 10$  cm on bulk mirrors; from bottom right to top left, perfect mirror (blue), silicon (green), and silica (red).

of the WKB phase:

$$S\phi(z) \equiv \frac{\phi'''(z)}{\phi'(z)} - \frac{3}{2} \left( \frac{\phi''(z)}{\phi'(z)} \right)^2. \quad (16)$$

This means that nonadiabatic processes are characterized by this Schwarzian derivative, similarly to nonadiabatic emission of photons in vacuum after reflection from moving mirrors [41,42].

It follows that the WKB approximation is good when the second term in  $\tilde{p}^2$  in (15) is much smaller than the first one. It can be shown that this is the case for the problem being studied in the present paper for short as well as long distances, which means that left- and rightward propagation are well defined in both limits. The nonadiabatic processes giving rise to quantum reflection occur in the intermediate distance range, and their efficiency is significant for large values of the quantity

$$Q(z) \equiv \frac{\hbar^2 S\phi}{2p^2} = \frac{\hbar^2 p'''(z)}{2 p(z)^3} - \frac{3\hbar^2}{4} \left( \frac{p''(z)}{p(z)^2} \right)^2. \quad (17)$$

The adiabatic approximation breaks down in regions where  $|Q(z)| \sim 1$ , which have been dubbed the *badlands*. Nonadiabatic quantum reflection happens there, where the notions of left- and rightward propagation are no longer well defined.

Figure 3 features the numerical evaluation of this badlands function  $Q(z)$  as a function of distance  $z$  to the wall (atomic units), for  $\bar{H}$  dropped from  $h = 10$  cm on perfect, silicon, or silica mirrors (the same color codes as in Figs. 1 and 2). The plots clarify two features which explain the apparent paradox discussed in the preceding section. First, quantum reflection occurs closer and closer to the wall for weaker and weaker CP-vdW interaction. Second, the value reached by  $Q(z)$  is thus larger and larger, since the CP interaction gets steeper and steeper when atoms approach the wall. When considered together, these two features explain why a weaker potential leads to a more efficient reflection than a stronger one. In fact, the quantum reflection probabilities  $|r|^2$  (see, for example, the numbers given in Table II) increase with increasing peak value of the badlands function  $Q(z)$ .

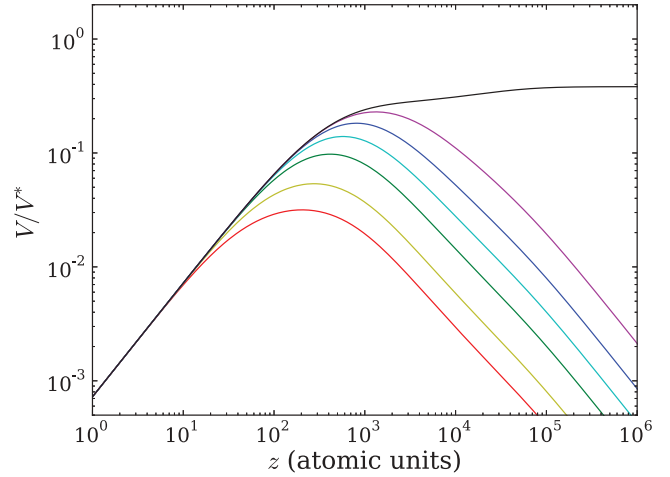


FIG. 4. (Color online) Casimir-Polder potential for  $\bar{H}$  in the vicinity of a silica slab, drawn as the ratio  $V/V^*$ ; from top to bottom, the thickness is infinite (black), 50 nm (magenta), 20 nm (deep blue), 10 nm (light blue), 5 nm (deep green), 2 nm (light green), and 1 nm (red).

## V. REFLECTION ON A THIN SLAB

This discussion suggests that one should try to weaken further the CP-vdW interaction with the aim of enhancing quantum reflection [20]. In the present section, we analyze this idea by studying either slabs having a finite thickness or a graphene layer.

The calculations proceed along the same lines as previously, except for the fact that slabs of finite thickness  $d$  have smaller reflection amplitudes than the corresponding bulk materials. There is a general relation between these amplitudes [33]:

$$\rho_{\text{slab}}^p = \frac{(1 - e^{-2Kd}) \rho_{\text{bulk}}^p}{1 - e^{-2Kd} (\rho_{\text{bulk}}^p)^2}. \quad (18)$$

When the CP-vdW interaction is calculated at distances  $z$  smaller than the thickness  $d$ , the results of the bulk are recovered. This can be understood from the fact that  $\rho_{\text{slab}}^p$  goes to  $\rho_{\text{bulk}}^p$  for large values of  $d$  (up to exponentially small corrections). In contrast, the long-distance behavior of the CP potential is completely changed because the exponential factor now plays an important role in (18). Even the power-law index is changed for the potential which now varies as

$$V(z) \xrightarrow{z \gg \ell, d} -\frac{C_5}{z^5}. \quad (19)$$

Figure 4 shows the exact CP-vdW potentials obtained from (2) for  $\bar{H}$  atoms on slabs of amorphous silica, with different values for the thickness  $d$ . All cases are drawn as ratios of  $V(z)$  with the same reference potential  $V^*$  already used in Fig. 1. The ratios tend to the same linear variations  $C_3z/C_4^*$  at small distances as for the silica bulk [bottom (red) curve in Fig. 1] and to inverse distance laws  $C_5/(C_4^*z)$  at large distances, with the value of  $C_5$  being proportional to  $d$ . This behavior can be expected from a simple argument where the potential  $V_{\text{slab}}(z)$  at distance  $z$  from a slab of thickness  $d$  is obtained from the difference  $V_{\text{bulk}}(z) - V_{\text{bulk}}(z + d)$  with  $V_{\text{bulk}}$  the potential at distance  $z$  from the bulk. The scaling given by this simple argument is correct while the value of  $C_5$  is not exact.

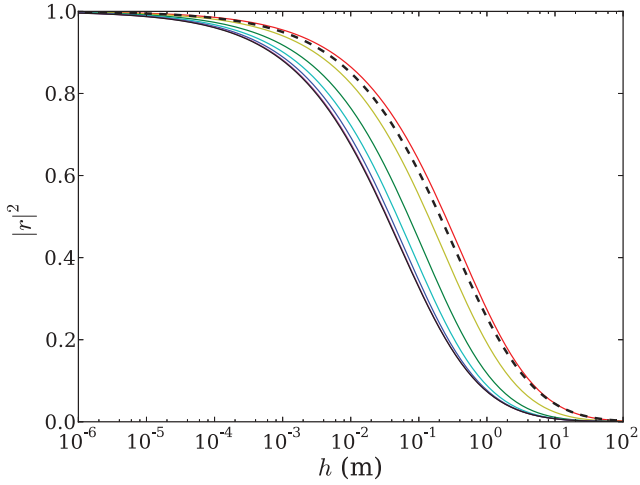


FIG. 5. (Color online) Quantum reflection probability  $|r|^2$  as a function of the free-fall height  $h$  for  $\bar{\text{H}}$  atoms on silica slabs; from bottom to top, the thickness is infinite (black), 50 nm (magenta), 20 nm (deep blue), 10 nm (light blue), 5 nm (deep green), 2 nm (light green), and 1 nm (red). The dashed line is the result for quantum reflection on nondoped graphene.

We depict in Fig. 5 the numerical solution for the quantum reflection probability obtained with the exact CP-vdW potentials for  $\bar{\text{H}}$  atoms falling onto silica slabs with various values of the thickness (the same color code as in Fig. 4). As expected, larger and larger values are obtained for the quantum reflection probability on thinner and thinner silica slabs, that is, also steeper and steeper CP-vdW potentials. For a free-fall height  $h \sim 10$  cm for example, the probability  $|r|^2$  reaches  $\sim 50\%$  for 3 nm slabs while it is only 33% for bulk silica. For comparison we also show the quantum reflection coefficient for graphene. Interestingly the same high quantum reflection as on a (not realistic) 1 nm slab can be obtained with the quantum reflection reaching 61% for nondoped graphene. This value increases only slightly ( $\leq 2\%$ ) if doping is included.

**VI. LOW-ENERGY LIMIT**

We finally discuss the limit of *near-threshold* quantum reflection, where the incident atomic energy  $E$  goes to zero. Quantum reflection is thus characterized by a scattering length [23] which we will calculate in the present section for the different cases discussed above, with the aim of optimizing applications for manipulating antihydrogen with material walls [34,35].

In order to conform to standard notation, we replace  $p$  by  $\hbar k$  in this section ( $k$  is not to be confused with the electromagnetic wave vector used in the beginning of this paper). The reflection amplitude  $r$  is a function of  $k$  which can be written in terms of a complex-valued function  $a(k)$  having the dimension of a length:

$$r(k) = -\exp[-2ika(k)]. \tag{20}$$

The real part of  $a(k)$  determines the phase at reflection while its imaginary part determines the quantum reflection

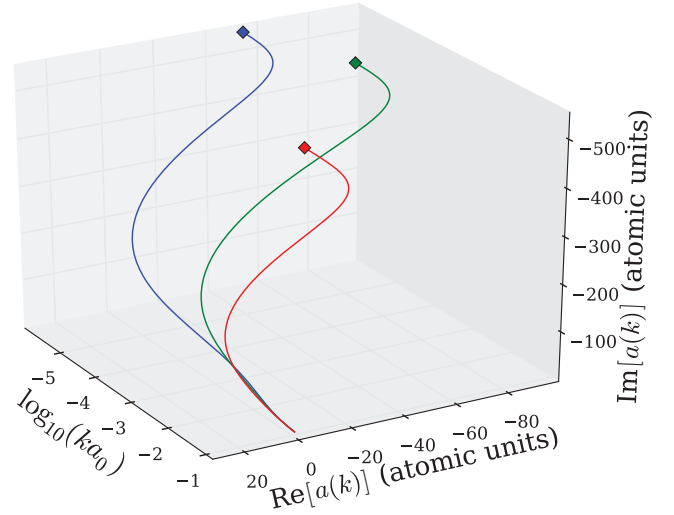


FIG. 6. (Color online) Three-dimensional representation of the variation of the real and imaginary parts of  $a(k)$  versus wave vector for  $\bar{\text{H}}$  atoms on bulk mirrors; from top left to bottom right, perfect mirror (blue), silicon (green), and silica (red).

probability:

$$|r|^2 = \exp\{4k\text{Im}[a(k)]\}. \tag{21}$$

We show in Fig. 6 the variations of real and imaginary parts of  $a(k)$  versus wave vector (measured in atomic units) for  $\bar{\text{H}}$  atoms falling onto a perfect mirror and bulk silicon and silica (the same color codes as in Fig. 2). We see that  $a(k)$  goes to a finite value  $a(0)$  when  $k \rightarrow 0$ , which is known as the scattering length; the values of  $a(0)$  are collected in Table III.

We also show in Fig. 7 the variations of the real and imaginary parts of  $a(k)$  versus wave vector (measured in atomic units) for  $\bar{\text{H}}$  atoms on silica slabs (the same color codes as in Fig. 5). Again,  $a(k)$  goes to a finite value  $a(0)$  when  $k \rightarrow 0$ , the real and imaginary parts of which are collected in Table IV.

We observe large variations of these values, which can have important applications for manipulating  $\bar{\text{H}}$  with material walls. By considering quantum gravitational traps for  $\bar{\text{H}}$  bounded below by the quantum reflection from the CP-vdW potential and above by gravity, one obtains the following lifetime for the quantum bouncer in the first gravitational quantum state [34]:

$$\tau = \frac{\hbar}{2mg |\text{Im} a(0)|}. \tag{22}$$

The lifetime is thus  $\sim 5$  times larger for thin silica slabs than for the perfect mirrors considered in the calculations of [34]. The same improvement holds for the width of resonances between

TABLE III. Real and imaginary parts of the scattering length  $a(0)$  for  $\bar{\text{H}}$  falling on perfect mirrors, bulk silicon and silica, and graphene (given in units of  $a_0$ ).

Perfect mirror		Silicon		Silica		Graphene	
Re( $a$ )	Im( $a$ )	Re( $a$ )	Im( $a$ )	Re( $a$ )	Im( $a$ )	Re( $a$ )	Im( $a$ )
-53.0	-543.0	-97.2	-435.2	-77.0	-272.6	-15.4	-109.7

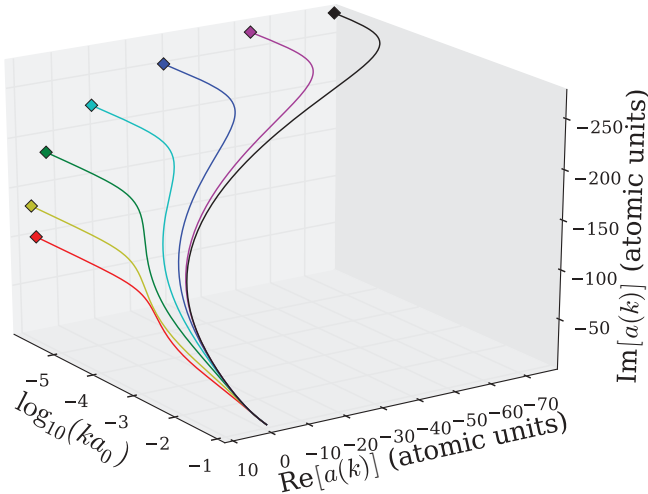


FIG. 7. (Color online) Three-dimensional representation of the variation of the real and imaginary parts of  $a(k)$  versus wave vector for  $\bar{\text{H}}$  atoms falling onto silica slabs; from top right to bottom left, the thickness is infinite (black), 50 nm (magenta), 20 nm (deep blue), 10 nm (light blue), 5 nm (deep green), 2 nm (light green), and 1 nm (red).

quantum states which can be used for precise spectroscopic determination of the energies of these states, a technique that could allow a better accuracy for the gravitational behavior of  $\bar{\text{H}}$  atoms in future experiments [35].

The same techniques could also allow the trapping of antiatoms above curved material surfaces and them guiding them at will during the longer lifetime achieved thanks to quantum reflection from steep potentials.

TABLE IV. Real and imaginary parts of the scattering length of antihydrogen on silicon and silica slabs (given in units of  $a_0$ ).

$d$ (slab thickness)	Silicon		Silica	
	$\text{Re}(a)$	$\text{Im}(a)$	$\text{Re}(a)$	$\text{Im}(a)$
1 nm	3.0	-178.1	6.5	-97.9
2 nm	1.6	-231.8	7.5	-130.3
5 nm	-6.5	-311.2	3.2	-181.9
10 nm	-21.8	-367.8	-9.3	-221.1
20 nm	-45.2	-408.0	-29.1	-250.1
50 nm	-73.1	-429.7	-53.3	-267.4
100 nm	-85.0	-433.7	-64.4	-271.2
Bulk	-97.2	-435.2	-77.0	-272.6

## VII. CONCLUSION

We have given realistic estimates of the VdW-CP potential above matter slabs of arbitrary thickness and the corresponding reflection probability for antihydrogen atoms. From our analysis we deduce that a substantial amount of quantum reflection is to be expected in the GBAR experiment. We have given a detailed analysis of the reflection process, solving the paradox of weaker potentials leading to higher reflection. Finally we have investigated the low-energy regime of quantum reflection and given quantitative predictions for the scattering length.

## ACKNOWLEDGMENTS

The authors thank the ESF Research Networking Program CASIMIR [43] and the GBAR Collaboration [44] for providing excellent possibilities for discussions and exchange.

- [1] J. Lennard-Jones and A. Devonshire, *Proc. R. Soc. London, A* **156**, 6 (1936); **156**, 29 (1936).
- [2] H. Casimir and D. Polder, *Nature (London)* **158**, 787 (1946); *Phys. Rev.* **73**, 360 (1948).
- [3] V. U. Nayak, D. O. Edwards, and N. Masuhara, *Phys. Rev. Lett.* **50**, 990 (1983).
- [4] J. J. Berkhout, O. J. Luiten, I. D. Setija, T. W. Hijmans, T. Mizusaki, and J. T. M. Walraven, *Phys. Rev. Lett.* **63**, 1689 (1989).
- [5] I. A. Yu, J. M. Doyle, J. C. Sandberg, C. L. Cesar, D. Kleppner, and T. J. Greytak, *Phys. Rev. Lett.* **71**, 1589 (1993).
- [6] F. Shimizu, *Phys. Rev. Lett.* **86**, 987 (2001).
- [7] V. Druzhinina and M. DeKieviet, *Phys. Rev. Lett.* **91**, 193202 (2003).
- [8] H. Oberst, Y. Tashiro, K. Shimizu, and F. Shimizu, *Phys. Rev. A* **71**, 052901 (2005).
- [9] V. P. A. Lonij, W. F. Holmgren, and A. D. Cronin, *Phys. Rev. A* **80**, 062904 (2009).
- [10] B. S. Zhao, H. C. Schewe, G. Meijer, and W. Schöllkopf, *Phys. Rev. Lett.* **105**, 133203 (2010).
- [11] T. A. Pasquini, Y. Shin, C. Sanner, M. Saba, A. Schirotzek, D. E. Pritchard, and W. Ketterle, *Phys. Rev. Lett.* **93**, 223201 (2004).
- [12] T. A. Pasquini, M. Saba, G. B. Jo, Y. Shin, W. Ketterle, D. E. Pritchard, T. A. Savas, and N. Mulders, *Phys. Rev. Lett.* **97**, 093201 (2006).
- [13] M. Berry and K. Mount, *Rep. Prog. Phys.* **35**, 315 (1972).
- [14] W. Brenig, *Z. Phys. B* **36**, 227 (1980).
- [15] D. P. Clougherty and W. Kohn, *Phys. Rev. B* **46**, 4921 (1992).
- [16] C. Henkel, C. Westbrook, and A. Aspect, *J. Opt. Soc. Am. B* **13**, 233 (1996).
- [17] C. Carraro and M. Cole, *Prog. Surf. Sci.* **57**, 61 (1998).
- [18] H. Friedrich, G. Jacoby, and C. G. Meister, *Phys. Rev. A* **65**, 032902 (2002).
- [19] H. Friedrich and J. Trost, *Phys. Rep.* **397**, 359 (2004).
- [20] T. E. Judd, R. G. Scott, A. M. Martin, B. Kaczmarek, and T. M. Fromhold, *New J. Phys.* **13**, 083020 (2011).
- [21] J. D. Perreault, M. Bhattacharya, V. P. A. Lonij, and A. D. Cronin, *Phys. Rev. A* **77**, 043406 (2008).
- [22] V. Druzhinina, M. Mudrich, F. Arnecke, J. Madroñero, and A. Buchleitner, *Phys. Rev. A* **82**, 032714 (2010).
- [23] A. Y. Voronin and P. Froelich, *J. Phys. B* **38**, L301 (2005); A. Y. Voronin, P. Froelich, and B. Zygelman, *Phys. Rev. A* **72**, 062903 (2005).

- [24] P. Pérez *et al.* (GBAR Collaboration), <http://gbar.in2p3.fr/public/SPSC-111025.pdf>
- [25] G. Feinberg and J. Sucher, *Phys. Rev. A* **2**, 2395 (1970).
- [26] M. Babiker and G. Barton, *J. Phys. A* **9**, 129 (1976).
- [27] J. M. Wylie and J. E. Sipe, *Phys. Rev. A* **30**, 1185 (1984).
- [28] J. F. Babb, G. L. Klimchitskaya, and V. M. Mostepanenko, *Phys. Rev. A* **70**, 042901 (2004).
- [29] K. A. Milton, *Am. J. Phys.* **79**, 697 (2011).
- [30] A. Lambrecht, P. A. Maia Neto, and S. Reynaud, *New J. Phys.* **8**, 243 (2006).
- [31] T. Emig, N. Graham, R. L. Jaffe, and M. Kardar, *Phys. Rev. Lett.* **99**, 170403 (2007).
- [32] R. Messina, D. A. R. Dalvit, P. A. Maia Neto, A. Lambrecht, and S. Reynaud, *Phys. Rev. A* **80**, 022119 (2009).
- [33] A. Lambrecht, I. Pirozhenko, L. Duraffourg, and P. Andreucci, *Europhys. Lett.* **77**, 44006 (2007).
- [34] A. Y. Voronin, P. Froelich, and V. V. Nesvizhevsky, *Phys. Rev. A* **83**, 032903 (2011).
- [35] A. Y. Voronin, V. V. Nesvizhevsky, and S. Reynaud, *Phys. Rev. A* **85**, 014902 (2012); *J. Phys. B* **45**, 165007 (2012).
- [36] Y. Zhang and D. P. Clougherty, *Phys. Rev. Lett.* **108**, 173202 (2012).
- [37] M. Marinescu, A. Dalgarno, and J. F. Babb, *Phys. Rev. A* **55**, 1530 (1997).
- [38] C. Koughia, S. Kasap, and P. Capper, *Springer Handbook of Electronic and Photonic Materials*, Springer Handbook Series (Springer, Berlin, 2006).
- [39] M. Bordag, I. V. Fialkovsky, D. M. Gitman, and D. V. Vassilevich, *Phys. Rev. B* **80**, 245406 (2009).
- [40] Kummer's  $M$  function is also known as the  ${}_1F_1$  hypergeometric function. It holds that  $M(\frac{3}{2}, 4, z) = -16L_{-3/2}^{(3)}(z)$  where  $L_n^{(\alpha)}$  is a generalized Laguerre polynomial. More information can be found at <http://dlmf.nist.gov>
- [41] S. Fulling and P. Davies, *Proc. R. Soc. London, A* **348**, 393 (1976).
- [42] A. Lambrecht, M.-T. Jaekel, and S. Reynaud, *Eur. Phys. J. D* **3**, 95 (1998).
- [43] <http://www.casimir-network.org>
- [44] <http://www.gbar.in2p3.fr>